ADVANCED MATERIALS
www.advmat.de

Top-Down Approach for Nanophase Reconstruction in Bulk Heterojunction Solar Cells

Jaemin Kong, In-Wook Hwang, and Kwanghee Lee**

Bulk-heterojunction (BHJ) polymer solar cells (PSCs) that have the potential for use as low-cost, lightweight and flexible energy harvesting sources have recently exhibited power conversion efficiencies (PCEs) exceeding 9% in laboratory-scale single-junction devices.[1,2] In the BHJ-based PSCs comprising photoactive blends of p-type electron donors (π-conjugated polymers) and n-type electron acceptors (fullerene derivatives), the device efficiency is significantly affected by the nanomorphology of BHJ photoactive layers because the size of nanoscale phase separation of donor and acceptor materials is directly associated with the dissociation probability of photoinduced excitons that have a short diffusion lengths of ~10 nm, and inter-percolation (i.e., bicontinuous pathways) of separated donor/acceptor-rich phases can significantly affect charge carrier transports.[3–5]

For the BHJ composites consisting of recently developed promising copolymers such as poly(thieno[3,4-b]thiophene-co-benzodithiophene)s (PTB7 derivatives) and fullerene derivatives, it has been tipically found that oversized fullerene aggregates with a size of several hundred nanometers in diameter were readily formed in as-cast polymer:fullerene BHJ composite films.[6–8] Traditional post-optimization processes such as thermal annealing[9] and solvent-vapor annealing[10] have no effect on or rather adversely affect the optimization of BHJ nanostrutures favorable for efficient charge transfer/transport, while the addition of a small amount of guest additive solvent (e.g., 1,8-diiodooctane, b.p. ≈ 365 °C at 760 mm Hg) into host solvent (e.g., chlorobenzene, b.p. ≈ 131 °C at 760 mm Hg) prior to film casting process[11] can suppress the formation of problematical massive fullerene-rich segregates which are usually found in the pristine BHJ film cast from additive-free pure solution, consequently leading to dramatic PCE enhancement of PSCs.[12–14]

Dr. J. Kong,[+] Prof. K. Lee
Heeger Center for Advanced Materials
Research Institute for Solar & Sustainable Energies
Gwangju Institute of Science & Technology
Gwangju 500–712, Republic of Korea
E-mail: klee@gist.ac.kr
Dr. I-.W. Hwang[+]
Advanced Photonics Research Institute
Gwangju Institute of Science & Technology
Gwangju 500–712, Republic of Korea
E-mail: hwangiw@gist.ac.kr
Prof. K. Lee
School of Materials Science & Engineering
Gwangju Institute of Science & Technology
Gwangju 500–712, Republic of Korea
[+]These authors contributed equally to this work.

DOI: 10.1002/adma.201402182

Although the simple 'additive-adding and film-casting' process is very effective to inhibit the occurrence of oversized fullerene-rich segregation, a vertical phase separation or surface segregation of specific component in vertical direction is still often detected in the BHJ films.[15–17] Because oversaturated component (usually polymers) upon film drying are forced to dispatch toward free interface to minimize the surface energy difference governed by the interaction between each component molecule and free/buried interface,[18–21] surface segregation can occasionally occur during the first evaporation stage (i.e., evaporation of lower-boiling-point host solvent) irrespective of the solvent-addtive action that is predominently exhibited in the second evaporation stage after the evaporation of majority of host solvent.[22] Moreover, the selective solubility of additive solvents for the fullerene can cause unexpected polymer aggregation already in additive-added solution,[22,23] and it might be possible to form overgrown polymer-nanoaggregates in the aged solution. A recent study additionally indicates that solvent additives, regardless of whether the additives can dissolve the polymers, presumably degrade host solvent quality to promote earlier polymer aggregation.[22] Therefore, a strategic approach to rule out the extraneous problems arising from the additive-adding to film-casting processes (e.g., overgrown polymer aggregates in solution or/and surface segregation of specific component in film) may further increase the genuine ability of processing additives for optimizing BHJ nanomorphologies, and thereby enhance the device performances.

Here, we report an unprecedented approach for re-constructing BHJ nanomorphologies in a top-down manner. In contrast to the conventional 'first-additive-adding and second-film-casting' procedure, we developed a new processing protocol of 'first-film-casting and second-additive-soaking', so-called post-additive soaking (PAS). By applying a specific solvent mixture containing a few traces of solvent additive (e.g., 1,8-diiodooctane) and most buffer solvents (e.g., hexane) onto already-cast pristine BHJ films via a simple rinsing treatment, oversized fullerene-rich clusters in the films are instantaneously disassembled and redistributed, resulting in finely re-mixed donor/acceptor nanophases. In particular, this PAS process enables a 3D compositional homogeneity (horizontally and vertically) without surface segregation, eventually resulting in highest power conversion efficiency (η_e = 9.74%) reported thus far for single-junction BHJ solar cells. Furthermore, this new processing protocol (i.e., PAS) can be widely applicable for various binary BHJ composites including conjugated polymers and even small-molecular systems within a short processing time (a few seconds), yielding comparable or even higher performances than those from conventional pre/post-optimization processes.

Scheme 1 representatively depicts top-down nanophase reconstruction via the PAS treatment. The bottom image was

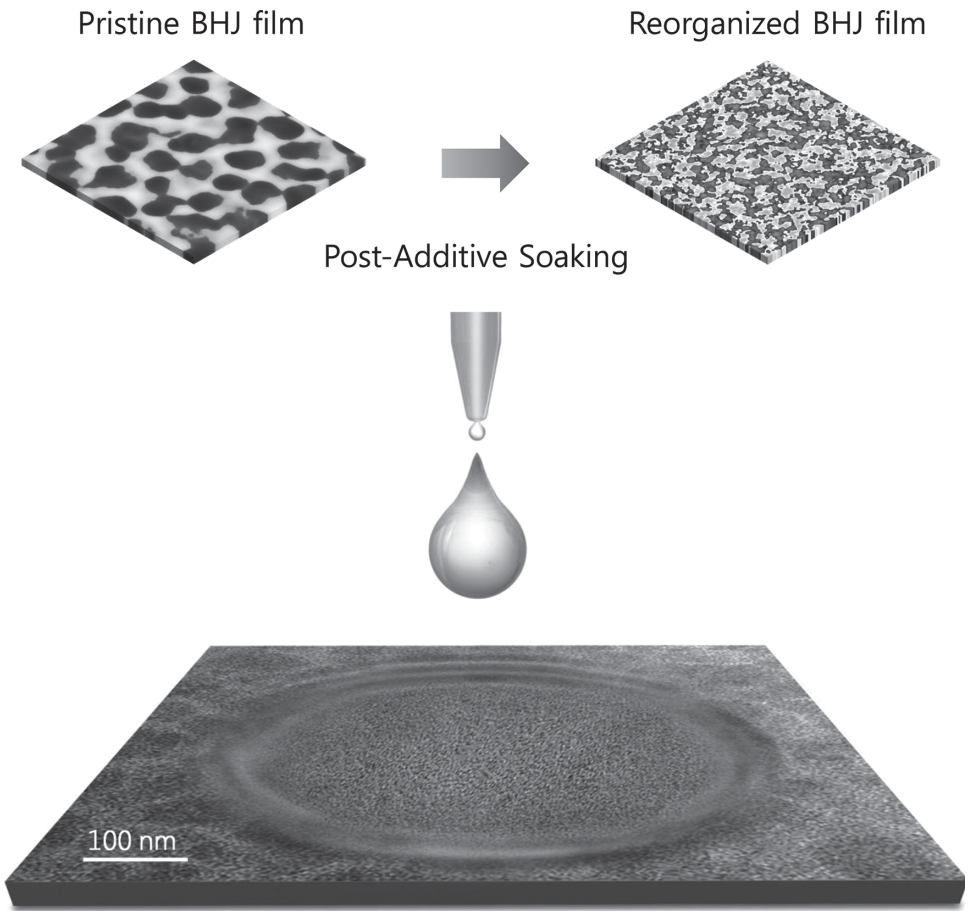

Scheme 1. Schematic view of the PAS-assisted top-down control of BHJ nanomorphology. The two top cartoons conceptually demonstrate the disassembling (i.e., top-down control) of oversized fullerene-rich segregates into smaller nanoaggregates by PAS. The bottom image, which was obtained by combining the experimental TEM data measured for the PTB7:$PC_{71}BM$ BHJ film before and after PAS, illustrates the facile PAS treatment, leading to the instantaneous and drastic morphology evolution in the solid state. In the figure, the bright and dark regions indicate polymer- and fullerene-rich domains, respectively.

combined with real transmittance electron microscope (TEM) images obtained from the BHJ composite using one of the highest performing copolymers of benzodithiophene-derivative, poly(thieno[3,4-b]thiophene-co-benzodithiophene) (PTB7) and a fullerene derivative, [6,6]-phenyl-C_{71} butyric acid methyl ester ($PC_{71}BM$) before and after PAS treatment. The pristine BHJ film apparently exhibited ~100 nm-sized fullerene-rich aggregates (dark regions) with poor connectivity. After the PAS treatment the fullerene-rich aggreagtes were disappeared, and the BHJ nanostructure underwent the morpholgical reconstruction resulting in highly percolated pathways as clearly shown in the TEM image (Scheme 1).

This dramatic change in nanomorphology instantaneously occurred when the pristine BHJ films were rinsed with a solvent mixture comprising a trace of well-known solvent additive such as 1,8-diiodooctane (DIO) and most buffer solvent. To directly feed the solvent additive (e.g., DIO) through the film surface without destroying the film shape, a choice of buffer solvent is very important. To be used as buffer solvent, the solvent basically must not dissolve both donor polymers and acceptor fullerene derivatives, but should be miscible with DIO. After tests with several kinds of solvents, nonpolar organic solvents such as n-hexane are empirically found to fully satisfy the aforementioned criteria. Optionally, octane or heptane can be used as a buffer solvent instead of n-hexane to control the feeding/soaking speed of processing additive via adjusting total vapor pressure of solvent mixtures. In order to help the solid-state BHJ film absorb the DIO, a certain amount of cyclohexane (acting as a marginal solvent for polymer) is also added in the solvent mixture as a second buffer solvent for weakly dissolving the film surface. We note that the buffer solvents chosen inhere may not be the best ones, but we try to find optimum mixing ratios of the selected solvents (please see experimental section and supplementary information for more details). During the PAS treatment, the buffer solvents (n-hexane and cyclohexane) prevented film destruction and weakly swelled the BHJ film, whereas the solvent additive (DIO) was instantaneously soaked from the film surface and seemingly redistributed the fullerene molecules in the film. These collaborative functions might enable the instantaneous reconstruction of BHJ nanomorphology in the film state.

Interestingly, the PAS treatment exhibits quite universal applicability with various BHJ binary systems using conjugated polymers and even small molecular systems (the details

Adv. Mater. **2014**,
DOI: 10.1002/adma.201402182

in Supplementary Information: Figure S1–4). Amongst them, in this report, we would focus on most efficient BHJ composite comprising a semiconducting copolymer poly[4,8-bis(5-(2-ethylhexyl)thiophen-2-yl)benzo[1,2-b:4,5-b']dithiophene-co-3-fluorothieno[3,4-b]thiophene-2-carboxylate] (PTB7-Th) and $PC_{71}BM$. **Figure 1** summarized morphological and compositional changes of PTB7-Th:$PC_{71}BM$ BHJ film (donor to acceptor ratio of 1:1.7) before/after PAS treatment. The PAS treatment was conducted with the previously optimized additive/buffer-solvent mixture [DIO/(cyclohexane:n-hexane) = 6/(29:71)] onto the 180 nm thickness pristine PTB7-Th:$PC_{71}BM$ films. Those films were spin-coated from the 27 mg/ml composite chlorobenzene solution at 450 rpm spinning rate, which is much slower than typical cases of ~2000 rpm (see experimental section, Figure S5–9, and Table S1–3). The PAS-treated films were characterized using atomic force microscopy (AFM), bright/dark field transmission electron microscopy (TEM) with energy-dispersive X-ray spectroscopy (EDS), time-of-flight secondary ion mass spectrometry (ToF-SIMS) and UV-Vis absorption spectroscopy.

The changes in surface morphology of BHJ film were characterized by AFM before/after PAS treatment as shown in Figure 1a and b. The pristine film (Figure 1a) that was obtained from additive-free pure host solvent (i.e., chlorobenzene) exhibited a rough surface topology (RMS roughness ≈ 3.4 nm) with large domains (average diameter of ~200 nm). Boundaries of the domains were more clearly found in phase image (inset of Figure 1a). After PAS treatment, the large domains have vanished off from the surface, and the film displayed much smoother topology (RMS roughness ≈ 1.0 nm), as shown in Figure 1b.

The large domains that have been detected in AFM for the pristine film might be attributed to the fullerene-rich regions from the following analysis of TEM data presented in Figure 1c and 1d, and Figure S10. This assignment was further supported by superimposing 2D elemental map of EDS on the dark-field TEM image (insets); the sky blue dot as a marker for sulfur element (S) in the EDS data was densely located in the dark area that reflected polymer-rich region in the dark-field image (inset of Figure 1c). When we deliberately increased the ratio of fullerene contents in the BHJ composites (1:3 of polymer:fullerene blend ratio), it was clearly indicated that polymers were concentrated in dark areas of dark-field TEM image (Figure S10b).

In the PAS-treated BHJ film, on the other hand, intermixing of polymer and fullerene components was significantly increased with finely interpenetrated channels of a size < 10 nm with the polymer fibrils in the fullerene matrix, as shown in Figure 1d. Notably, one could also find the hierarchical nanostructures that have previously been suggested by Chen et al.[24] as an ideal nanomorphology in the similar BHJ system of PTB7:$PC_{61}BM$ composite. In the dark-field TEM image (inset of Figure 1d) polymer fibrils and fullerenes were found in the range from several nanometers to tens of nanometers, which simultaneously percolated each other in the polymer-rich and fullerene-rich domains of hundreds of nanometers in size.

For a detailed compositional impact of PAS treatment on vertical direction, we conducted ToF-SIMS depth profiling of both BHJ films. The ToF-SIMS depth profiles, obtained by plotting the S^- (m/q = 34) and C^- signals (m/q = 12) as a function of the sputtering time to quantify the relative concentration of the polymer and fullerene molecules, provide clear evidence of the drastic redistribution of component materials throughout the films upon PAS treatment (Figure 1e and 1f). In the Figure 1e, the pristine BHJ film exhibits a sharp S^- peak in the initial period (t < 100 s), which might be indicative of PTB7-Th segregates formed at the film surface. Because of the lower surface energy of PTB7-Th compared to that of $PC_{71}BM$ (Figure S11), PTB7-Th would be accumulated at the film surface and minimize the surface energy difference.[18–21] Recently, Hedley et al. showed that large domains of 100 – 200 nm in diameter incorporating small sphere-like fullerene aggregates of tens of nanometer in diameter were covered or enveloped with the "skin" layer in PTB7:$PC_{71}BM$ blend film.[25] Because the both polymers, PTB7 in the literature and PTB7-Th used in our study have very similar molecular structure and properties, we can analogize that the sharp peak of S^- signals on the film surface (Figure 1e) might be attributed to the skin layer that mainly consist of the segregated polymers.

In the PAS-treated film, however, the initial sharpe S^- peak has disappeared, as observed in Figure 1f. The PAS-treated film did not exhibit any local segregation of specific components (i.e., the absence of sharp ToF-SIMS peaks), which might contribute to the improved performance of the PAS-treated devices by improving charge carrier transports to the electrodes and minimizing carrier-trapped sites. The overall nanomorphology of PAS-treated films might be predominantly determined by the movement of fullerenes due to their good solubility in DIO, whereas the already-solidified polymer domains might be passively reconstructed. The fullerene dissolved in the DIO might float together with the solvent evaporation and percolate into already-solidified (but less-ordered) polymer chains preformed at the film surface. In Figure 1f, one can also find somewhat crossed compositional gradation of each component in a vertical direction. As evaporating DIO from the film surface, the fullerene molecules dissolved in the DIO could be floated together with the direction of evaporation at the initial stage of the evaporation. However, the DIO solvent molecules evaporated to the free surface might induce the concentration gradient of the fullerene in the DIO-soaked wet film in the vertical direction, so that the concentration gradient of fullerene upon drying can reversely dispatch the fullerene into less fullerene-concentrated bottom side. In addition, because the solidified fullerene molecules might reduce the total surface energy with the buried interface, the enrichment of fullerene near the bottom side can be further promoted. Therefore, polymer chains might be relatively pushed toward top side of the film to form the final depth profiles (Figure 1f). The enriched donor polymers and acceptor fullerenes near the anode and cathode, respectively, might provide superior pathways for the holes and electrons to the corresponding electrodes in inverted PSC.[16,17,26]

The absorption spectrum measurements also illustrate that the PAS treatment changes the polymer ordering and material composition of the BHJs, as illustrated in Figure 1g and 1h. PAS leads to decreased absorption intensity of the BHJ at 350–550 nm, whereas the absorption between 550–800 nm increases (Figure 1g). The decreased absorption feature in the

ADVANCED MATERIALS
www.advmat.de

Materials Views
www.MaterialsViews.com

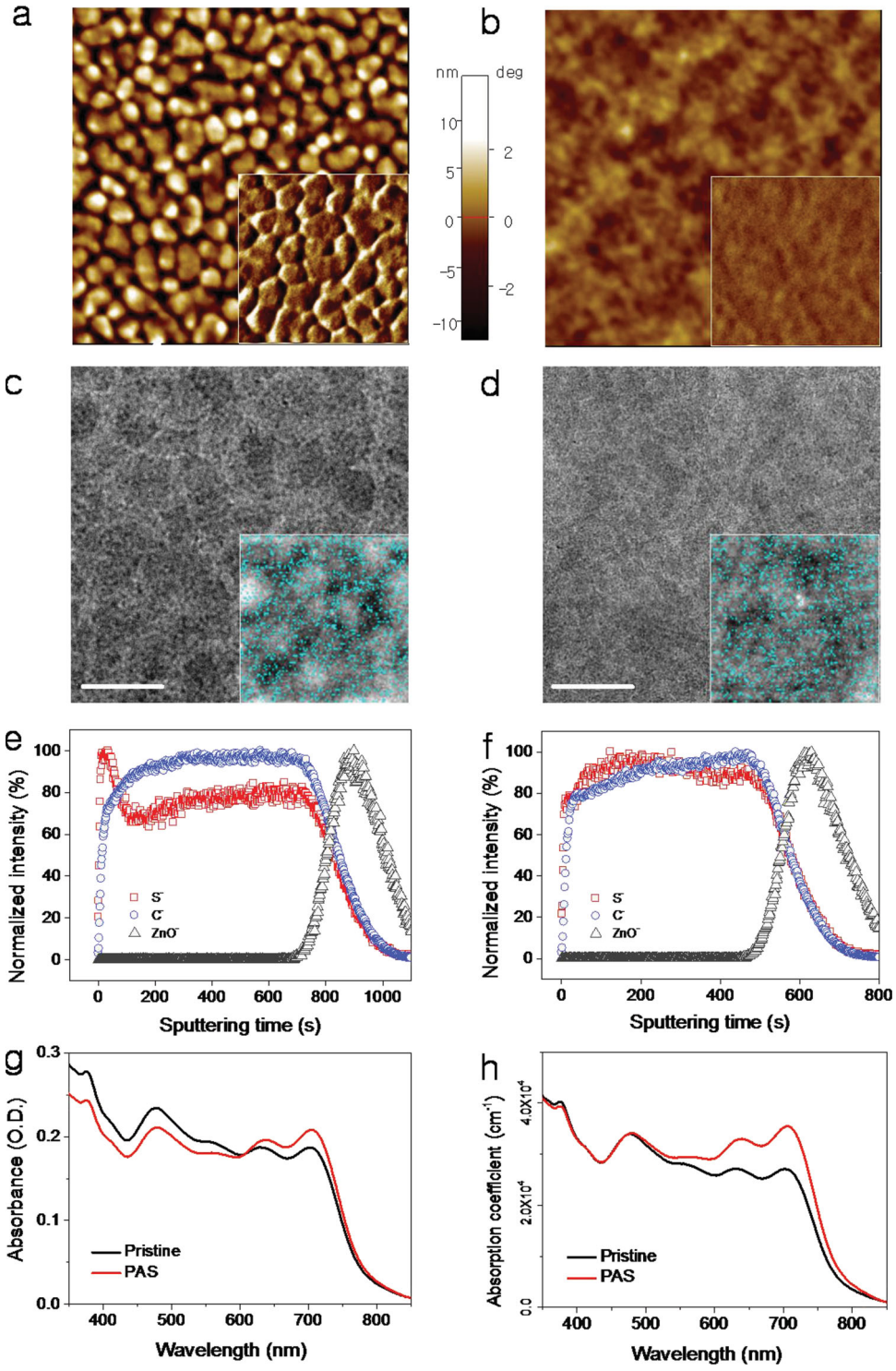

Figure 1. Nanomorphology change of the PTB7-Th:$PC_{71}BM$ BHJ film before and after PAS. Tapping mode AFM topography images (5 μm × 5 μm) obtained for the BHJ film before (a) and after (b) PAS; the insets show the corresponding AFM phase images (2.5 μm × 2.5 μm). Bright field TEM images obtained before (c) and after (d) PAS. The dark and bright regimes indicate fullerene- and polymer-rich domains, respectively. The scale bar represents 200 nm. The insets show dark-field TEM images, which are superimposed with a 2D elemental sulfur (S) map obtained using energy-dispersive X-ray spectroscopy (EDS); the sky blue dots represent sulfur (S) atoms that solely exist in the PTB7-Th polymer. In-depth compositional distributions of the BHJ film before (e) and after (f) PAS, which were obtained using a ToF-SIMS depth profiler. The BHJ samples were prepared on ZnO-coated glasses. Transmission-type absorption (g) and corresponding absorption coefficient spectra (h) obtained from the BHJ film before (black line) and after (red line) PAS.

Adv. Mater. **2014**,
DOI: 10.1002/adma.201402182

short wavelength region originates from the removal of $PC_{71}BM$ during PAS, which is consistent with the ~20 nm reduction of the film thickness (Figure S11). We empirically observed that the deliberate removal of the $PC_{71}BM$ from the BHJ results in superior PCEs, presumably because of the removal of surplus fullerene molecules. For the absorption coefficient spectra, the PAS-treated film spectrum exhibited an amplified polymer absorption coefficient in the long-wavelength regime (Figure 1h). This feature is indicative of the enhanced intermolecular π-π stacking of PTB7-Th polymer chains, which is consistent with previous reports, and is also supported by grazing incidence (GI) X-ray diffraction data (Figure S13).[2,27,28]

To assess the impact of the nanomorphological changes after the PAS treatment on photoelectrical performance, we use the BHJ films with/without the PAS treatment as the photoactive layer in photovoltaic device. The photovoltaic characteristics were investigated using an inverted PSC architecture with a structure of ITO/ZnO/PTB7-Th:$PC_{71}BM$/MoO_x/Ag. **Figure 2**a and 2b present the device structure and energy level diagram, in which photo-excited electrons and holes are collected at the cathode (ITO) and anode (Ag), respectively. Figure 2c presents current density-voltage (*J*-*V*) profiles measured under a simulated 1.5 G irradiation with 100 mW cm^{-2}. The device fabricated using the pristine PTB7-Th:$PC_{71}BM$ (black line) exhibits a PCE of 5.76%, with an open-circuit voltage (V_{OC}) of 0.81 V, short-circuit current (J_{SC}) of 12.7 mA cm^{-2}, and fill-factor (FF) of 0.56. In contrast, the device with the PAS-treated PTB7-Th:$PC_{71}BM$ (red line) exhibits significantly enhanced device parameters (PCE ≈ 9.56%, V_{OC} ≈ 0.79 V, J_{SC} ≈ 17.79 mA cm^{-2}, and FF ≈ 0.68), as summarized in **Table 1**.

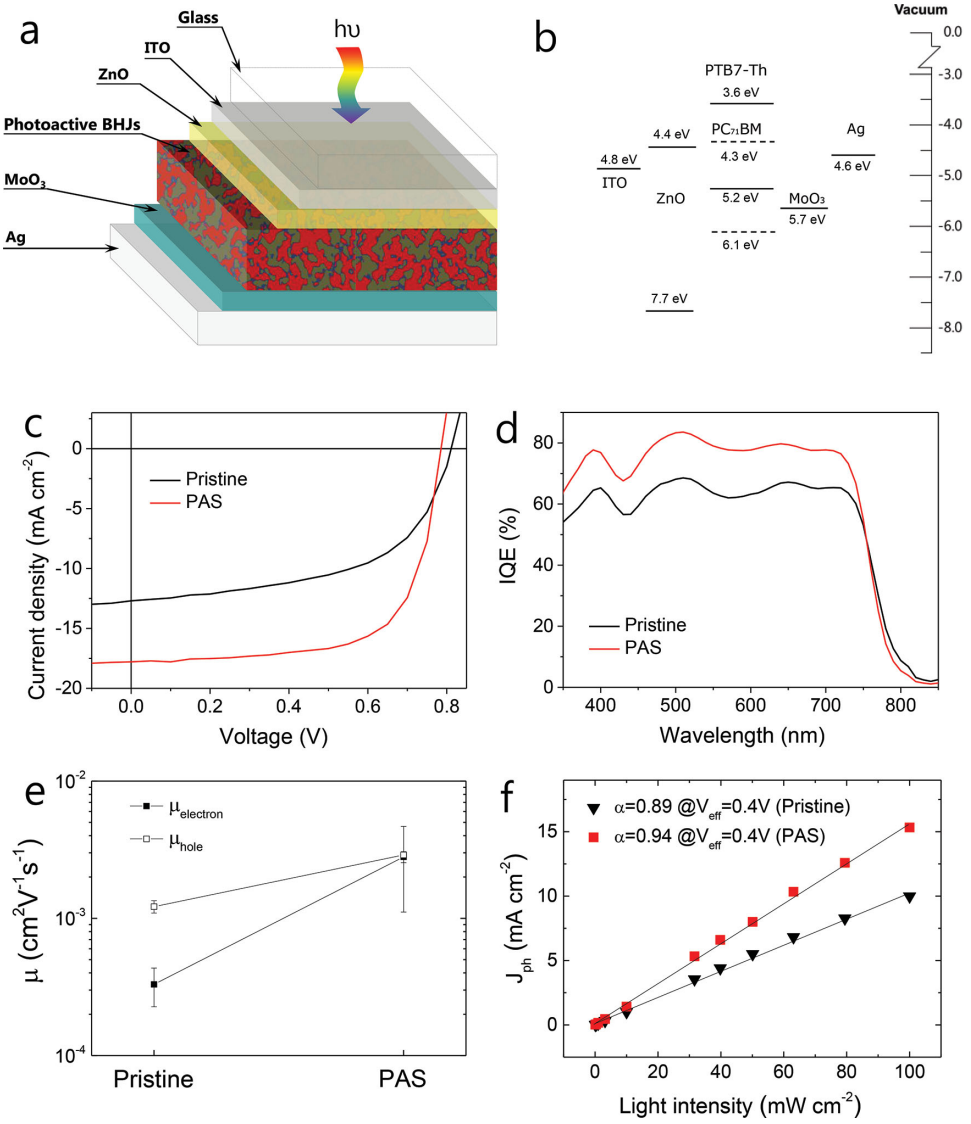

Figure 2. Effect of PAS on electrical and photovoltaic performances. (a) Schematic view of the fabricated inverted SC and (b) corresponding energy level diagram. Comparison of photovoltaic and electrical properties before (black) and after (red) PAS: (c) photovoltaic *J*-*V* plots, (d) internal quantum efficiency spectra, (e) hole and electron mobility characterized by SCLC measurements and (f) photocurrents plotted as a function of irradiation light intensity.

Table 1. Photovoltaic device parameters obtained from various PSCs fabricated from different kinds of BHJ materials with respect to several optimization methods.

		V_{OC} [V]	J_{SC} [mA cm^{-2}]	FF	PCE* [%]
P3HT: PCBM	Pristine	0.63	3.95	0.41	1.02
	PAS	0.61 (0.61)	8.64 (8.40)	0.68 (0.67)	3.58 (3.43)
	Thermal annealing	0.60 (0.60)	8.29 (8.20)	0.66 (0.64)	3.28 (3.15)
P3HT: ICBA	Pristine	0.86	7.19	0.56	3.46
	PAS	0.83 (0.84)	10.08 (9.81)	0.66 (0.65)	5.52 (5.36)
	Solvent annealing	0.84 (0.83)	9.97 (9.84)	0.64 (0.62)	5.36 (5.06)
PCPDTBT: $PC_{71}BM$	Pristine	0.66	10.2	0.47	3.16
	PAS	0.55 (0.56)	12.90 (12.53)	0.56 (0.56)	3.97 (3.93)
	Pre-additive adding	0.56 (0.57)	12.90 (12.49)	0.55 (0.55)	3.97 (3.92)
PTB7: $PC_{71}BM$	Pristine	0.75	10.91	0.47	3.84
	PAS	0.72 (0.73)	15.15 (14.80)	0.74 (0.74)	8.07 (7.99)
	Pre-additive adding	0.73 (0.73)	14.02 (13.80)	0.72 (0.71)	7.37 (7.15)
PTB7-F20: $PC_{71}BM$	Pristine	0.71	9.17	0.38	2.47
	PAS	0.67 (0.68)	15.0 (14.1)	0.61 (0.61)	6.13 (5.85)
	Pre-additive adding	0.67 (0.68)	13.8 (13.5)	0.63 (0.61)	5.82 (5.60)
PTB7-Th: $PC_{71}BM$	Pristine	0.81	12.70	0.56	5.76
	PAS	0.79 (0.79)	17.79 (17.8)	0.68 (0.67)	9.56 (9.42)
	Pre-additive adding	0.80 (0.79)	16.76 (17.0)	0.69 (0.67)	9.25 (9.00)
p-DTS(FBTTh$_2$)$_2$:$PC_{71}BM$	Pristine	0.79	7.60	0.52	3.12
	PAS	0.78 (0.77)	11.73 (11.86)	0.69 (0.66)	6.31 (6.03)
	Pre-additive adding	0.80 (0.80)	11.88 (11.84)	0.58 (0.55)	5.51 (5.21)

*The device parameters show the best values of each BHJ type. Numbers in parentheses are the average values of 8 cells of each type.

In parallel with the *J-V* characteristics, the internal quantum efficiency (IQE), which is defined as the ratio of collected charge carriers to absorbed photons, displays a ~33% enhancement over the broad spectral range of 350–750 nm (Figure 2d). The IQE spectra were obtained by dividing the incident photon-to-current efficiency (IPCE) spectra by the total absorption spectra measured at 1-reflection (Figure S14). The IQE spectra are predominantly affected by the overall carrier dynamics, such as the exciton diffusion efficiency (η_{ED}), charge transfer efficiency (η_{CT}), and charge collection efficiency (η_{CC}).[29] Because the electron transfer efficiency from a p-type polymer to n-type fullerene is known to be close to unity ($\eta_{CT} \approx 100\%$),[30] η_{ED} and η_{CC} may dominantly affect the IQE. The η_{ED} is known to be associated with the obtainable exciton generation rate (G),[31] which is proportional to the number of excitons that diffuse to the interface of n- and p-type materials. G for the BHJs was determined using the formula, $J_{ph} = eGL$,[32] where J_{ph} is the photocurrent density under a short-circuit condition, e is the elementary charge, and L is the active layer thickness. G for the PAS-treated BHJ was calculated to be ~7.1×10^{27} m^{-3} s^{-1}, which is 60% higher than that for the pristine BHJ (~4.4×10^{27} m^{-3} s^{-1}). This result implies a significant enhancement in η_{ED} caused by PAS, principally in good agreement with the finer nanonetworks shown in Figure 1d.

Space charge limited current (SCLC) measurements for characterizing the charge carrier transport along the vertical direction were performed (Figure S15). The SCLC analysis also confirms that our PAS treatment leads to electron mobility enhancement by a factor of ~10, resulting in similar mobility for the hole and electron, as illustrated in Figure 1e and Figure S15. In addition to charge carrier transport, charge recombination also affects the η_{CC}.[31,33] To investigate charge recombination, we plotted the photocurrents as a function of irradiation light intensity (Figure 2f and S16). By fitting the data with a power law function,[34,35] $J_{ph} \propto P^{\alpha}$, where P and α are the power generation rate and ideality factor, respectively, we obtained $\alpha \approx 0.89$ and 0.94 for the pristine and PAS-treated BHJ cells, respectively. The value of $\alpha \approx 0.94$, which is closer to unity, implies a reduction in the carrier recombination and space charge build-up of the PAS-treated cell, probably contributing to a higher η_{CC}.

In practical perspective, the PAS treatment is particularly of benefit to controlling nanomorphology regardless of whether preformed films are cast from different kind of solvents. Although the pristine BHJ films cast from very volatile solvents such as chloroform (b.p. ~ 61 °C) and from environment-friendly non-halogenated solvents such as o-xylene (b.p. ~ 144 °C) exhibit different nanomorphology (Figure S17), they presumably undergo similar nanomorphology evolution by the same PAS treatment, consequently resulting in increased device efficiencies by a factor of ~ 3.5 and ~ 2.3 respectively in the PAS-treated PSCs, as summarized in **Figure 3**a and **Table 2**.

Adv. Mater. **2014**,
DOI: 10.1002/adma.201402182

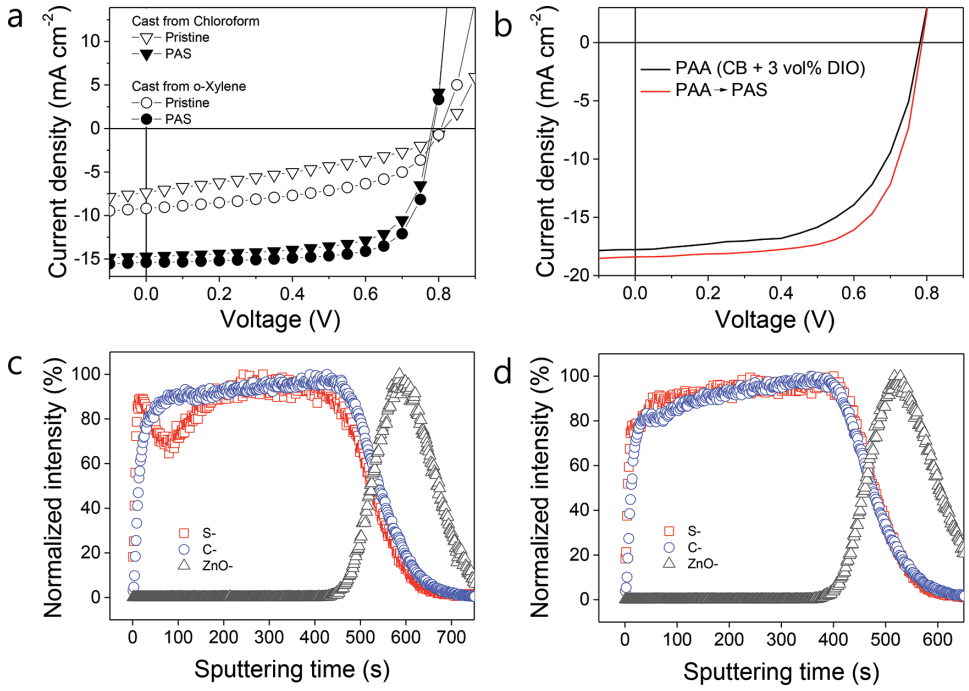

Figure 3. Universal and further photovoltaic PCE enhancements by PAS. (a) *J-V* profiles observed for the PSCs comprising PTB7-Th:$PC_{71}BM$ composites cast from volatile CF (reversed triangles) and less-volatile o-xylene (circles) solvents before (open symbols) and after (filled symbols) PAS. (b) *J-V* profiles for the PSC comprising the conventional-DIO-added-solution-processed PTB7-Th:$PC_{71}BM$ composite before (black) and after (red) PAS. ToF-SIMS depth profiles corresponding to the conventional DIO-processed PTB7-Th:$PC_{71}BM$ composite before (c) and after (d) PAS.

The preformed-film-independence might provide a broad processing spectrum of film casting condition because the nanomorphology can be independently controlled regardless of the state of preformed films by different processing conditions. It also means that some BHJ films having suboptimized nanomorphology can be further optimized by the PAS treatment. As shown in Figure 3b, indeed, when we conducted the PAS treatment on the 'less-optimized' thick BHJ film fabricated by conventional additive process (i.e., casting from 3 vol% DIO-added CB solution), 'more-optimized' device efficiency ($\eta_e \approx$ 9.74%) was obtained, which is the highest PCE, to our best knowledge, reported to date amongst BHJ-based single PSCs. In Figure 3c and 3d, the suboptimized film cast from conventional pre-additive-adding protocol exhibited an initial sharp S^- peak (at t < 100 s) in the ToF-SIMS depth profile, whereas the PAS-treated optimized film showed a continuous distribution of component materials without local segregation; thus elimination of the abrupt compositional fluctuation near the suface might contributed likely to the improved PCE.

Table 2. Photovoltaic device parameters obtained from PSCs comprising PTB7-Th:$PC_{71}BM$ composites fabricated from volatile (CF), less-volatile (o-xylene), and pre-additive-added (PAA) solutions before and after PAS.

Casting solution	treatment	V_{OC} [V]	J_{SC} [mA cm^{-2}]	FF	PCE [%]*
CF	Pristine	0.82	7.35	0.37	2.23
	PAS	0.78 (0.78)	14.73 (14.70)	0.69 (0.67)	7.93 (7.68)
o-Xylene	Pristine	0.80	9.19	0.51	3.75
	PAS	0.79 (0.78)	15.39 (15.34)	0.73 (0.72)	8.88 (8.61)
CB + 3vol%DIO	Pristine	0.78	17.77	0.60	8.31
	PAS	0.79 (0.78)	18.40 (18.41)	0.67 (0.66)	9.74 (9.48)

*The device parameters show the best values. Numbers in parentheses are the average values of 8 cells of each case.

The PAS treatment can be widely applicable for various BHJ composites from polymer:fullerene to small molecule:fullerene by altering the kind of processing additive (Table 1). In terms of the solvent additives used for PAS, DIO was observed to be effective for the BHJ composites containing a large proportion of fullerenes and weakly ordered polymers, such as PTB7:$PC_{71}BM$, PTB7-F40:$PC_{71}BM$, PTB7-Th:$PC_{71}BM$, and PCPDTBT:$PC_{71}BM$ (Figure S1–4). On the other hand, 1-chloronaphthalene (CN) that can dissolve both donor polymer and acceptor fullerene is more adaptable than DIO for optimizing BHJs, in which the blending ratio of donor to acceptor is greater than one, or the molecular packing of semi-crystalline donor polymer/small molecule significantly governs entire nanostructures, such as P3HT:PCBM, P3HT:ICBA, and *p*-DTS(FBTTh$_2$)$_2$:$PC_{71}BM$ (Figure S1–4). However, the criteria of mixing protocols are still unclear; thus additional controlled studies are goning to understand the mechanism of actions according to the processing additives.

In conclusion, we have demonstrated a top-down control technique for the reconstruction of BHJ nanomorphologies in the solid film state via a post-addtive soaking approach. By rinsing as-cast BHJ films with an additive/buffer solvent mixture, we could put off the action of processing additives after film solidification, helping a selective action of the processing additive especially on the problematical fullerene aggregates on

the as-cast films. In addition, this process promoted a 3D compositional homogeneity (in both horizontal and vertical direction) without surface segregation that was often found even in BHJ films processed from a conventional additive protocol (i.e., additive-adding and film-casting). Together with the conventional bottom-up optimization approaches, we believe that our top-down control technique may provide a bilateral pathway for optimizing various organic binary composites.

Experimental Section

Materials: The donor polymers and small molecule, i.e., poly(3-hexylthiophene) (**P3HT**), poly[2,6-(4,4-bis-(2-ethylhexyl)-4H-cyclopenta [2,1-B;3,4-B'] dithiophene)-alt-4,7(2,1,3-benzothiadiazole)] (**PCPDTBT**), polythieno[3,4-b]thiophene/benzodithiophene (**PTB7**), polythienothiophene-co-benzodithiophenes (**PTB7-F20**), poly[4,8-bis(5-(2-ethylhexyl) thiophen-2-yl)benzo[1,2-b:4,5-b']dithiophene-co-3-fluorothieno[3,4-b] thiophene-2-carboxylate] (**PTB7-Th**), and 7,79-(4,4-bis(2-ethylhexyl)-4H-silolo[3,2-b:4,5-b9]dithiophene-2,6-diyl)bis(6-fluoro-4-(59-hexyl-[2,29-bithiophen]-5-yl)benzo[c][1,2,5]thiadiazole) (**p-DTS(FBTTh$_2$)$_2$**) were purchased from 1-Material, Inc. The acceptor fullerene derivatives, i.e., phenyl-C61-butyric acid methyl ester (**PCBM**), indene-C60 bisadduct (**ICBA**), and phenyl-C71-butyric acid methyl ester (**PC$_{71}$BM**), were purchased from Nano-C, Inc. All of the solvents, including the solvent additives, were purchased from Sigma-Aldrich.

Spin-Cast Solution Preparation: The PTB7-Th:PC$_{71}$BM (1:1.7) composite was dissolved in chlorobenzene (CB) and stirred at room temperature for 12 h. The concentrations of PTB7-Th/CB and PC$_{71}$BM/CB were 10 and 17 mg/mL, respectively. This parent solution was separated into two vials for preparing additive-free and additive-added solutions, respectively. The 30 μL of DIO was added to a 1 mL parent solution to prepare the conventional additive-added solution.

PAS Reagent Preparation: The buffer solvent was composed of two non-halogenated aliphatic solvents, i.e., cyclohexane and n-hexane. The mixing ratio of the two solvents used to optimize the PTB7-Th:PC$_{71}$BM was 29:71 for cyclohexane:n-hexane and was empirically deduced from various attempts on the PTB7:PC$_{71}$BM composites. The amount of DIO added to the buffer solvent was adjusted based on the BHJ film thickness. In total, 2–4 vol% of DIO was added to the buffer solvent to optimize thin BHJ films with thicknesses of < 100 nm, whereas 4–8 vol% of DIO was added to the buffer solvent to optimize thicker films with thicknesses of 100–200 nm (Figure S9). At too high concentration of DIO above ~10%, the fullerenes were found to be excessively removed from the BHJ films.

BHJ Film Preparation: The pristine and conventional-additive-processed BHJ films were prepared by spin-casting the DIO-free and DIO-added composite solutions, respectively. The PAS-treated BHJ films were obtained by rinsing the dried pristine BHJ films with an optimal PAS reagent of DIO/(n-hexane:cyclohexane), whose ratio was adjusted based on the film thickness. The BHJ films were spin cast on several types of substrates to characterize the nanomorphologies and optical and electrical properties. The films were spin cast on fused silica substrates to measure the UV-Vis absorption and GI-XRD spectra and spin cast on ZnO-deposited ITO substrates to fabricate inverted-shape solar cells. After characterizing the solar cell performances, the same cells or films were used again to characterize the top-surface properties (by AFM) and in-depth compositional distribution (by ToF-SIMS depth profiling). The BHJ films were spin cast on heavily doped p-type silicon wafers coated with SiO_2 and on ultrathin carbon-sheet layered copper grids (#300 mesh, PELCO) to measure the charge carrier mobility (by TFT) and in-plane TEM images, respectively. PAS was also conducted on BHJ-coated TEM grid substrates.

BHJ Film Characterization: The contact angles were measured using a contact angle analyzer (SEO Phoenix-300 Touch). The film surface topography and phase images were measured under the AFM tapping mode (NanoFocus, Inc.). The depth profiles for the material distribution were obtained using a TOF-SIMS (ION-TOF, Germany) instrument. To sputter the device from the BHJ film surface, 1 keV Cs^+ ions were used (sputtering area: 300 μm × 300 μm), whereas a 30 keV Bi_3^+ beam was employed to analyze the composition distribution along the vertical direction, acquiring mass-to-charge ratios (m/q) of negatively charged secondary ions, e.g., C^- (m/q = 12), S^- (m/q = 32), ZnO^- (m/q = 80), from the analysis area (100 μm × 100 μm) centered at the sputtered region. The TEM images were obtained using a high-resolution transmission electron microscope (HR-TEM, JEOL JEM-3000) operating at 300 kV. Elemental 2D mapping was also conducted using STEM-EDS mapping and analysis of the same instrument. Transmission and 1-reflection absorption (1-R) spectra were obtained using a spectrometer (PerkinElmer Lambda 900). The GI-XRD spectra were measured using D8 ADVANCE with DAVINCI (BRUKER, Germany) with a LYNXEYE XE detector (2 theta = 2–50°).

Solar Cell Fabrication and Characterization: The patterned ITO-glass substrates were cleaned by sonication in distilled water, acetone, and IPA in sequence and dried overnight in an oven at 70 °C before fabricating solar cells with an inverted architecture of ITO(100 nm)/ZnO(20 nm)/PTB7-Th:PC$_{71}$BM(180 nm)/MoO_x(10 nm)/Ag(120 nm). The ZnO precursor solution prepared following Ref. [36] was used to deposit a ZnO layer (an electron transport layer) onto the ITO. The ZnO-coated substrates were dried at 150 °C for 40 min and transferred into a N_2-filled glove box. The pristine and conventional DIO-processed BHJ films were deposited on the ZnO by spin-casting respective DiO-free and DIO-added composite solutions at 450 rpm for 100 s. The PAS-treated BHJ films were obtained by spin casting the PAS reagents (solvent mixtures) onto the pristine BHJ film at 3,000 rpm. The BHJ-coated substrates were transferred to a vacuum chamber, where MoO_x (a hole transport layer) and Ag (an anode) were sequentially deposited using a thermal evaporator operating at ~5×10^{-7} torr. The photoactive area of 4.64 mm^2 was achieved using a shadow mask. The devices were finally encapsulated with a ~1 mm thickness slide glass using a 5-min epoxy paste. The *J-V* profiles were measured using a Keithley 236 source measure unit (SMU) under illumination with an incident light intensity of 100 mW cm^{-2} (300 W Newport-Oriel AM 1.5G light source) calibrated using a standard silicon reference cell (91150V, Oriel Instruments). External quantum efficiency (EQE) spectra were obtained using an IPCE measurement system (PV Measurements, Inc.). The mismatch of the J_{SC} values obtained from the *J-V* and IPCE data was negligible.

SCLC Device Fabrication and Characterization: For electron-only devices, a device structure of ITO/polyethyleneimine(~5 nm)/BHJ/LiF(~1 nm)/Al(~200 nm) was used. For hole-only devices, a structure of ITO/PEDOT:PSS(~15 nm)/BHJ/MoO_3(~10 nm)/Ag(~200 nm) was used. SCLC measurements were conducted using Keithley 236 Source Meter Unit. Measurements for electron mobility were performed in forward bias; bottom ITO side was positively biased. Measurements for hole mobility were performed in reverse bias; top siver side was positively biased.

Supporting Information

Supporting Information is available from the Wiley Online Library or from the author.

Acknowledgements

We would like to thank Alan J. Heeger for his comments on this work. We thank the Research Institute of Solar Energy (RISE) and Heeger Center for Advanced Materials (HCAM) at Gwangju Institute of Science and Technology (GIST) and the Korean Basic Science Institute in Daejeon and in Jeonju for the instruments used to fabricate the devices and characterize the morphologies. This research was financially supported by the Core Technology Development Program for Next-generation Solar Cells at the Research Institute for Solar and Sustainable Energies

DOI: 10.1002/adma.201402182

(RISE) in GIST and by the National Research Foundation of Korea (NRF) grant funded by the Korean government (MSIP) (No. 2008–0062606, CELA-NCRC). I.W. Hwang acknowledges the financial support from the Advanced Photonics Research Institute (APRI) Research Program from the Basic Science Research Program of GIST, Grant No. 2011–0006563 from the National Research Foundation funded by the Korean government Ministry of Education, Science, and Technology and the EI Project ARQ20114000114 (401–112–014) funded by the Korean Ministry of Environment.

Received: May 15, 2014
Revised: June 21, 2014
Published online:

[1] Z. He, C. Zhong, S. Su, M. Xu, H. Wu, Y. Cao, *Nat. Photonics* **2013**, *6*, 591.
[2] S.-H. Liao, H.-J. Jhuo, Y.-S. Cheng, S.-A. Chen, *Adv. Mater.* **2013**, *25*, 4766.
[3] G. Yu, J. Gao, J. C. Hummelen, F. Wudl, A. J. Heeger, *Science* **1995**, *270*, 1789.
[4] P. E. Shaw, A. Ruseckas, Ifor, D. W. Samuel, *Adv. Mater.* **2008**, *20*, 3516.
[5] H. Wang, H.-Y. Wang, B.-R. Gao, L. Wang, Z.-Y. Yang, X.-B. Du, Q.-D. Chen, J.-F. Song, H.-B. Sun, *Nanoscale* **2011**, *3*, 2280.
[6] J. S. Moon, C. J. Takacs, S. Cho, R. C. Coffin, H. Kim, G. C. Bazan, A. J. Heeger, *Nano Lett.* **2010**, *10*, 4005.
[7] Y. Liang, Z. Xu, J. Xia, S.-T. Tsai, Y. Wu, G. Li, C. Ray, L. Yu, *Adv. Mater.* **2010**, *22*, E135.
[8] M.-S. Su, C.-Y. Kuo, M.-C. Yuan, U-S. Jeng, C.-J. Su, K.-H. Wei, *Adv. Mater.* **2011**, *23*, 3315.
[9] W. Ma, C. Yang, X. Gong, K. Lee, A. J. Heeger, *Adv. Funct. Mater.* **2005**, *15*, 1617.
[10] G. Li, V. Shrotriya, J. Huang, Y. Yao, T. Moriarty, K. Emery, Y. Yang, *Nat. Mater.* **2005**, *4*, 864.
[11] J. Peet, J. Y. Kim, N. E. Coates, W. L. Ma, D. Moses, A. J. Heeger, G. C. Bazan, *Nat. Mater.* **2007**, *6*, 497.
[12] S. J. Lou, J. M. Szarko, T. Xu, L. Yu, T. J. Marks, L. X. Chen, *J. Am. Chem. Soc.* **2011**, *133*, 20661.
[13] B. A. Collins, Z. Li, J. R. Tumbleston, E. Gann, C. R. McNeill, H. Ade, *Adv. Energy Mater.* **2013**, *3*, 65.
[14] H.-C. Liao, C.-C. Ho, C.-Y. Chang, M.-H. Jao, S. B. Darling, W.-F. Su, *Mater. Today* **2013**, *16*, 326.
[15] L. Ye, Y. Jing, X. Guo, H. Sun, S. Zhang, M. Zhang, L. Huo, J. Hou, *J. Phys. Chem. C* **2013**, *117*, 14920.
[16] M. Kim, J.-H. Kim, H. H. Choi, J. H. Park, S. B. Jo, M. Sim, J. S. Kim, H. Jinnai, Y. D. Park, K. Cho, *Adv. Energy Mater.* **2014**, *4*, 1300612.
[17] X. Guo, M. Zhang, W. Ma, L. Ye, S. Zhang, S. Liu, H. Ade, F. Huang, J. Hou, *Adv. Mater.* **2014**, *24*, 4043.
[18] D. S. Germack, C. K. Chan, R. J. Kline, D. A. Fischer, D. J. Gundlach, M. F. Toney, L. J. Richter, D. M. DeLongchamp, *Macromolecules* **2010**, *43*, 3828.
[19] C. M. Björström, A. Bernasik, J. Rysz, A. Budkowski, S. Nilsson, M. Svensson, M. R. Andersson, K. O. Magnusson, E. Moons, *J. Phys.: Condens. Matter* **2005**, *17*, L529.
[20] S. Y. Heriot, R. A. L. Jones, *Nat. Mater.* **2005**, *4*, 782.
[21] D. S. Germack, C. K. Chan, B. H. Hamadani, L. J. Richter, D. A. Fischer, D. J. Gundlach, D. M. DeLongchamp, *Appl. Phys. Lett.* **2009**, *94*, 233303.
[22] N. Shin, L. J. Richter, A. A. Herzing, R. J. Kline, D. M. DeLongchamp, *Adv. Energy Mater.* **2013**, *3*, 938.
[23] K. Schmidt, C. J. Tassone, J. R. Niskala, A. T. Yiu, O. P. Lee, T. M. Weiss, C. Wang, J. M. J. Fréchet, P. M. Beaujuge, M. F. Toney, *Adv. Mater.* **2014**, *26*, 300.
[24] W. Chen, T. Xu, F. He, W. Wang, C. Wang, J. Strzalka, Y. Liu, J. Wen, D. J. Miller, J. Chen, K. Hong, L. Yu, S. B. Darling, *Nano Lett.* **2011**, *11*, 3707.
[25] G. J. Hedley, A. J. Ward, A. Alekseev, C. T. Howells, E. R. Martins, L. A. Serrano, G. Cooke, A. Ruseckas, I. D. W. Samuel, *Nat. Commun.* **2013**, *4*, 1.
[26] F. Liu, Y. Gu, J. W. Jung, W. H. Jo, T. P. Russell, *J. Polym. Sci. Pt. B-Polym. Phys.* **2012**, *50*, 1018.
[27] J. M. Szarko, J. Guo, Y. Liang, B. Lee, B. S. Rolczynski, J. Strzalka, T. Xu, S. Loser, T. J. Marks, L. Yu, L. X. Chen, *Adv. Mater.* **2010**, *22*, 5468.
[28] M. R. Hammond, R. J. Kline, A. A. Herzing, L. J. Richter, D. S. Germack, H.-W. Ro, C. L. Soles, D. A. Fischer, T. Xu, L. Yu, M. F. Toney, D. M. DeLongchamp, *ACS Nano* **2011**, *5*, 8248.
[29] S. H. Park, A. Roy, S. Beaupré, S. Cho, N. Coates, J. S. Moon, D. Moses, M. Leclerc, K. Lee, A. J. Heeger, *Nat. Photonics* **2009**, *3*, 297.
[30] A. C. Mayer, S. R. Scully, B. E. Hardin, M. W. Rowell, M. D. McGehee, *Mater. Today* **2007**, *10*, 28.
[31] V. D. Mihailetchi, L. J. A. Koster, J. C. Hummelen, P. W. M. Blom, *Phys. Rev. Lett.* **2004**, *93*, 216601.
[32] P. W. M. Blom, V. D. Mihailetchi, L. J. A. Koster, D. E. Markov, *Adv. Mater.* **2007**, *19*, 1551.
[33] A. Moliton, J.-M. Nunzi, *Polym. Int.* **2006**, *55*, 583.
[34] L. J. A. Koster, V. D. Mihailetchi, H. Xie, P. W. M. Blom, *Appl. Phys. Lett.* **2005**, *87*, 203502.
[35] A. J. Moulé, K. Meerholz, *Appl. Phys. B* **2008**, *92*, 209.
[36] Y. Sun, J. H. Seo, C. J. Takacs, J. Seifter, A. J. Heeger, *Adv. Mater.* **2011**, *23*, 1679.